Supporting Information

Distributed Feedback Lasers by Thermal Nanoimprint of Perovskites Using Gelatin Gratings

Isabel Allegro, Víctor Bonal, Emil R. Mamleyev, José M. Villalvilla, José A. Quintana, Qihao Jin, María A. García-Díaz*, Uli Lemmer**

Corresponding Authors

*isabel.allegro@kit.edu
*maria.diaz@ua.es
*uli.lemmer@kit.edu

Figure S1. ASE measurements of reference unpatterned perovskite film S2
Figure S2. Contact angle measurements S2
Figure S3. Imprint process S3
Figure S4. Surface of a pristine perovskite film S3
Figure S5. SEM images of stamp after four imprints S3
Figure S6. Lasing emission from DFB laser fabricated in the second imprint round S4
Figure S7. Comparison of this work's threshold with reported thresholds S4
Table S1. Summary of reported solution processed perovskite DFB film S4
Figure S8. Coupling coefficient as a function of the duty cycle S5
Figure S9. Calculation of the effective refractive index of the laser modes S5

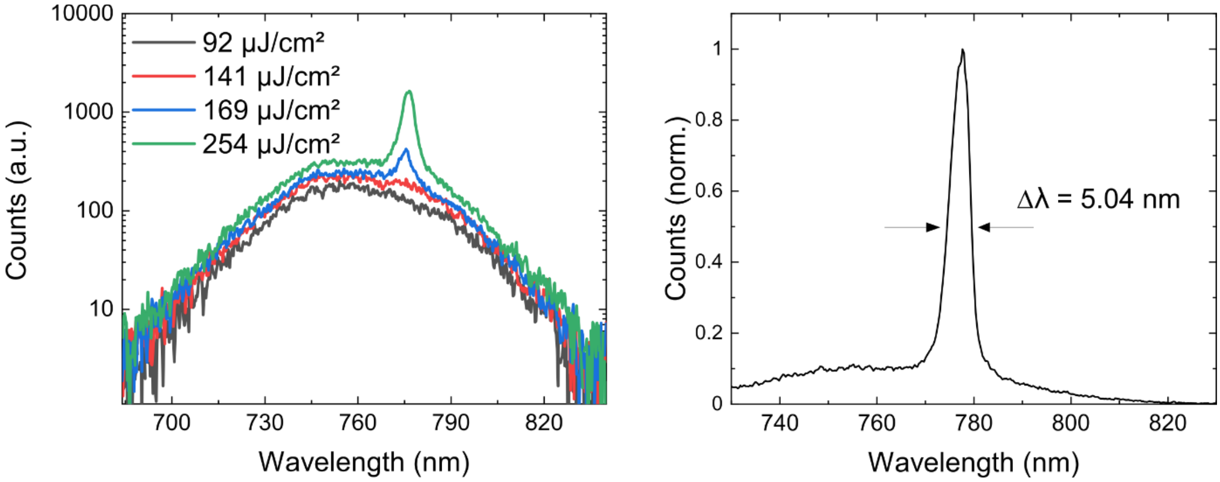

Figure S1. Amplified spontaneous emission (ASE) measurements on a reference unpatterned perovskite thin film spin-coated on glass. Emission spectra below and above threshold (left) and high-resolution spectrum of the ASE peak (right)

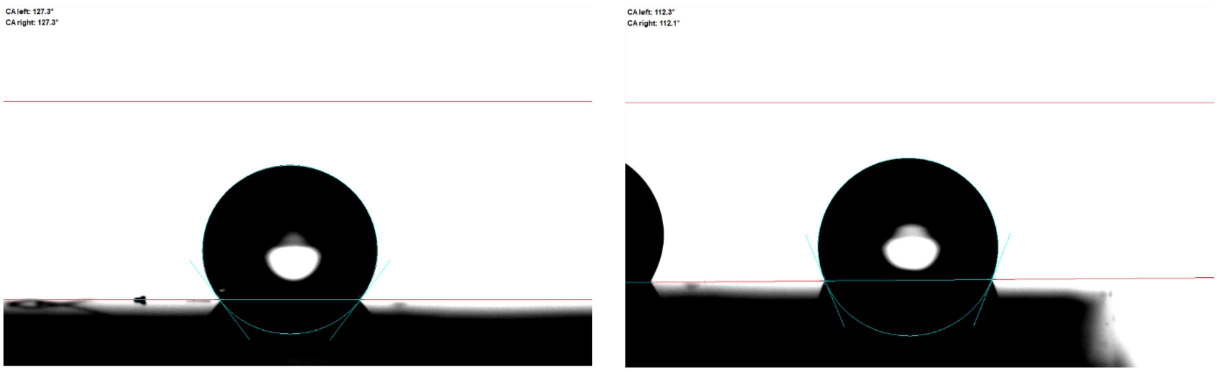

Figure S2. Contact angle measurement of the dichromated gelatin (DCG) stamp with anti-adhesion layer. Measurements at the center of the stamp (left) shows a higher hydrophobicity with a contact angle of 127.3° than at the edge of the stamp (right) with a contact angle of 112.2°.

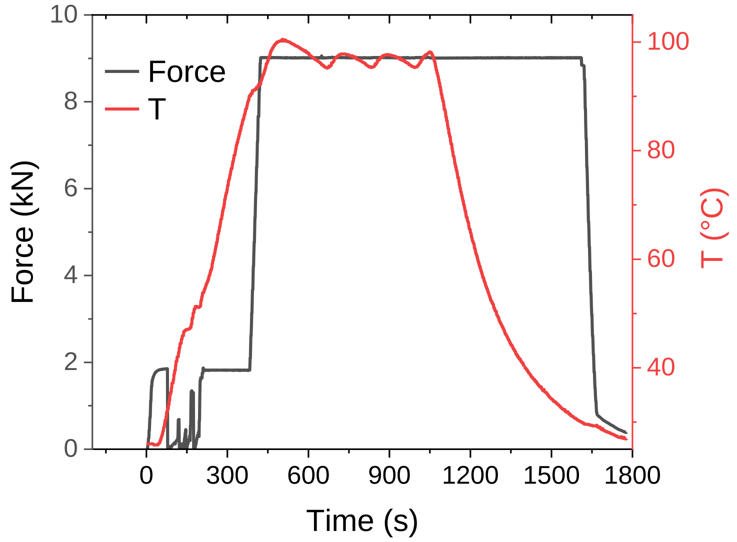

Figure S3. Force (black line) and temperature (red line) measured during the imprint process as a function of time. The used stamps have an area of 10 x 10 mm² so that a force of 9 kN corresponds to a pressure of 90 MPa.

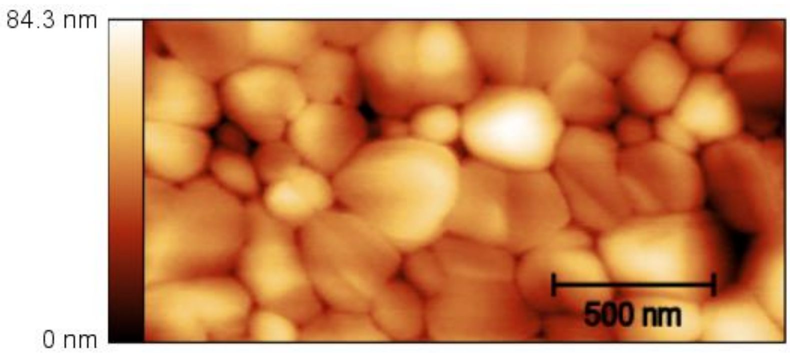

Figure S4. AFM image of the surface of a pristine perovskite film. Roughness RMS = 12.8 nm (over the 1 µm x 2 µm area).

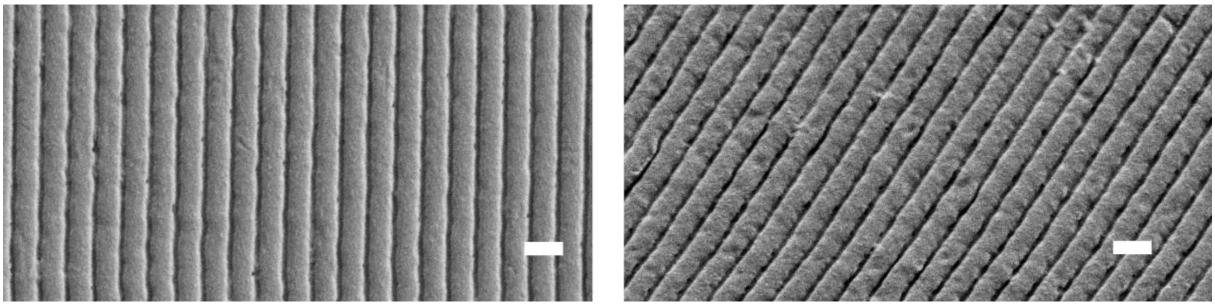

Figure S5. SEM images of DCG stamp after four imprint procedures. SEM image from the top (left) and with a 30° inclination (right), scale bars correspond to 500 nm.

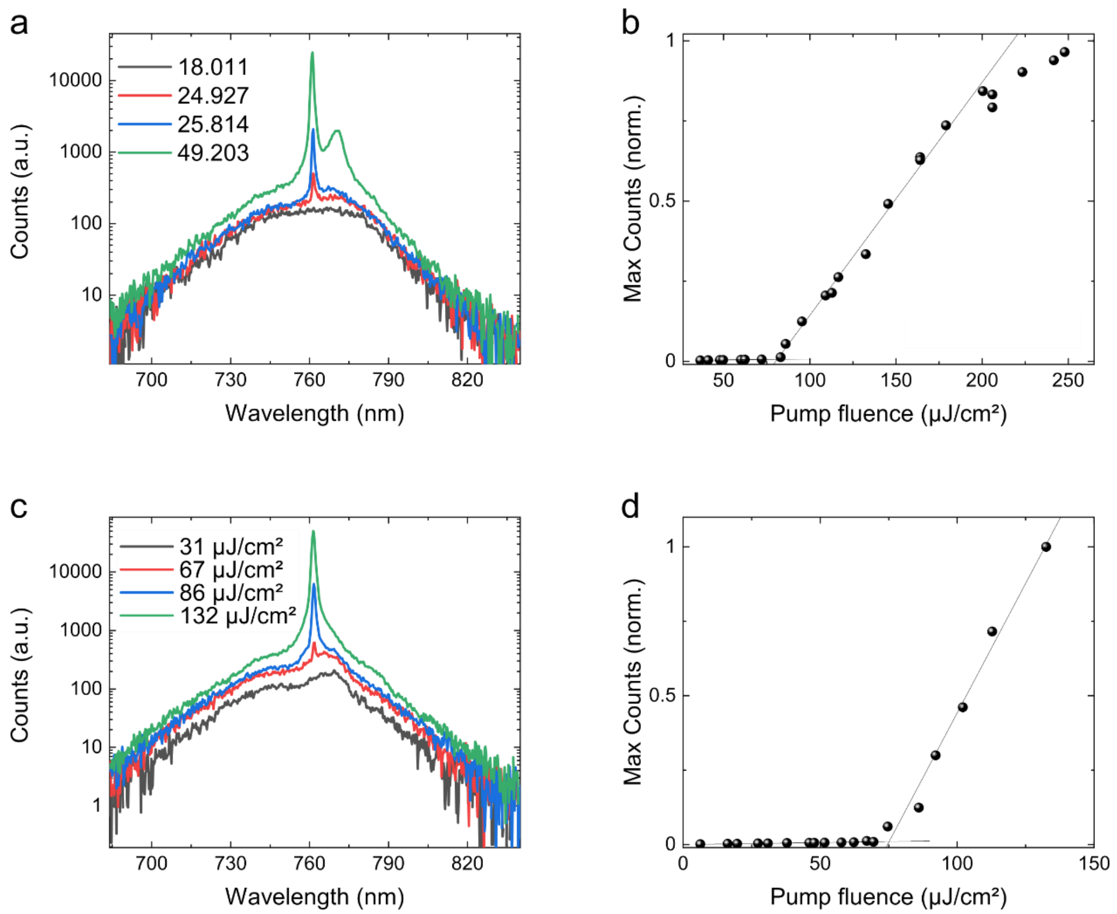

Figure S6. Comparison of lasing emission of perovskite DFB lasers fabricated in the first and second round of imprints. Emission spectra below and above threshold a) and c), and input-output characteristics of laser emission b) and d). Laser fabricated in the first round of imprint a) and b) exhibits a threshold of 81 μJ/cm² and laser fabricated in the second round of imprint (with the same stamp) exhibits a threshold of 75 μJ/cm². A quantitative measurement of the power conversion efficiency is quite challenging as we are working with low input pulse energies, but we estimated a value of less than 1%.

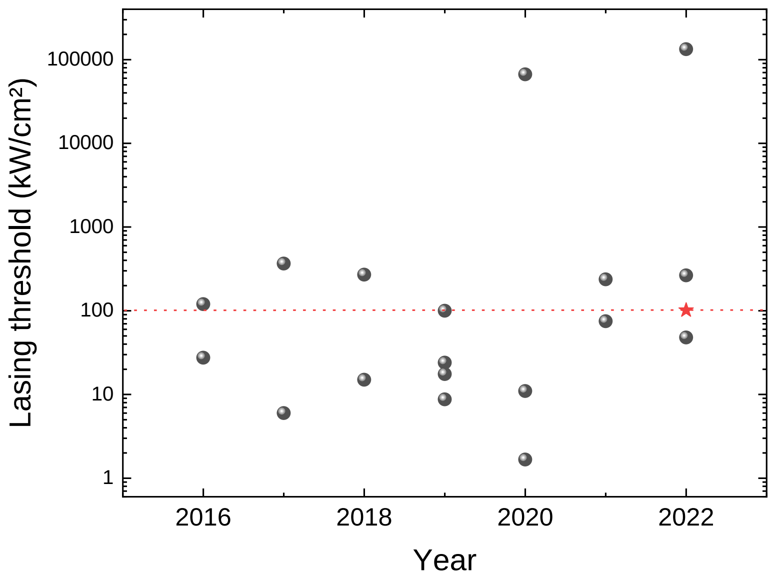

Figure S7. Summary of reported laser thresholds over the years (from Table S1) converted to kW/cm² by considering the excitation pulse width. The result from this paper is marked with a red star and the red dotted line provides a guide line.

Table S1. Summary of reported solution processed perovskite 2nd order DFB lasers.

Material	Threshold	Pump laser		Year	Ref
$Cs_{0.1}(MA_{0.17}FA_{0.83})Pb_{0.84}(I_{0.8}Br_{0.2})_{2,68}$	81 μJ cm^{-2}	532 nm	1 ns	2022	This work
$MAPbI_3$	240 μJ cm^{-2}	532 nm	5 ns	2022	[1]
$MAPbBr_3$	4.5 mJ/cm² +	355 nm	17 ns	2022	[2]
$MAPbBr_3$	20 μJ/cm²	400 nm	150 fs	2022	[3]
$MAPbBr_3$	47 μJ cm^{-2}			2021	[4]
$MAPbI_3$, $MAPbBr_3$, $MAPb(IBr)_3$	3 - 9.5 μJ cm^{-2}	532/355 nm	40 ps	2021	[5]
$(NMA/PEA)_2FA_{n-1}Pb_nBr_{3n+1}$	45/59 W cm^{-2} 5/33 μJ cm^{-2}	488 nm 337 nm	CW 3 ns	2020	[6]
$PEA_2FA_3Pb_4Br_{13}$	10 μJ cm^{-2}	400 nm	150 fs	2020	[7]
$CsPbBr_3$	7.2 μJ cm^{-2}	355 nm	0.3 ns	2019	[8]
$CsMAPb(IBr)_3$	4 μJ cm^{-2}	355 nm	40 ps	2019	[9]
$MAPbI_3$	7 μJ cm^{-2}	337 nm	0.8 ns	2019	[10]
$MAPbI_3$	14 μJ cm^{-2}	337nm	0.8 ns	2019	[11]
$MAPbI_3$	75 μJ cm^{-2}	532nm	5 ns	2018	[12]
$MAPbI_3$	270 μJ cm^{-2}	532 nm	1ns	2018	[13]
$CsPbBrI_2$	33 μJ cm^{-2}	355 nm	90ps	2017	[14]
$MAPbI_3$	17 kWcm^{-2} x	445 nm	CW	2017	[15]
$MAPbBr_3$	6 μJ/cm²	355 nm	1ns	2017	[16]
$MAPbI_3$	110 μJ/cm²	450 nm	4ns	2016	[17]
$MAPbI_3$	120 μJ/cm²	532 nm	1ns	2016	[18]

+ 260K

x 160K

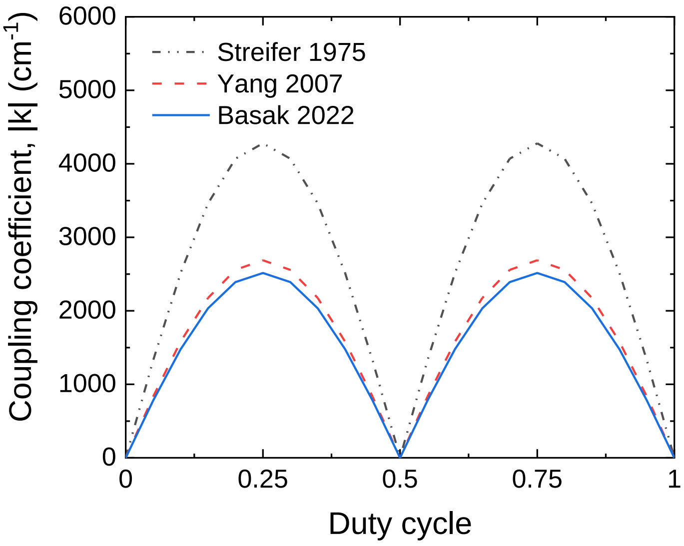

Figure S8. Coupling coefficient for a square grating as a function of the grating's duty cycle. The three curves correspond to the calculation of the coupling coefficient as a function of duty cycle using the equations in the referenced papers[1,19,20] and applying the perovskite refractive index (and our specific grating parameters).

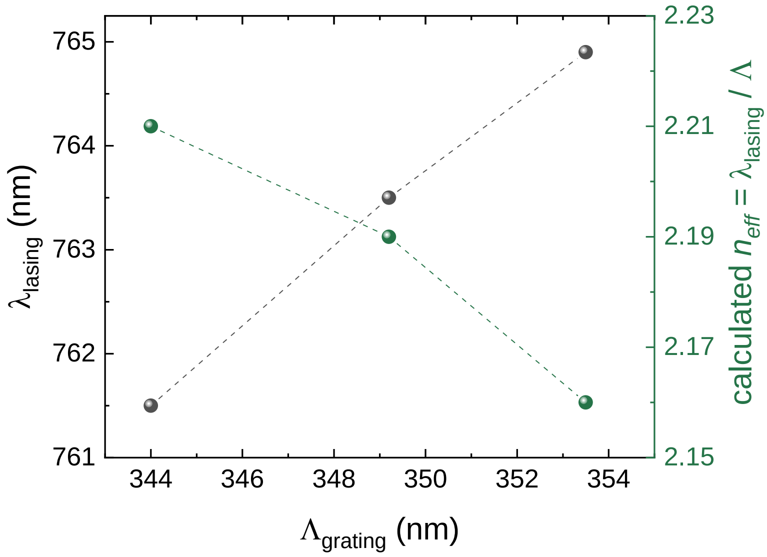

Figure S9. Wavelength of the lasing peak as a function of the grating period (black spheres and dashed line), and the corresponding effective refractive index of the lasing mode (green spheres and dashed line). The effective index n_{eff} is calculated from the experimental data by $n_{\mathrm{eff}} = \lambda_{\mathrm{lasing}} / \Lambda_{\mathrm{grating}}$.

References

1. Basak, S., Bar-On, O., and Scheuer, J. (2022) Metal-halide perovskite-based edge emitting lasers. *Opt. Mater. Express*, **12** (2), 375.

2. Moon, J., Alahbakhshi, M., Gharajeh, A., Li, Q., Li, Z., Haroldson, R., Kwon, S., Hawkins, R., Kim, M.J., Hu, W., Zhang, X., Zakhidov, A., and Gu, Q. (2022) Quasi-CW Lasing from Directly Patterned and Encapsulated Perovskite Cavity at 260 K. *ACS Photonics*, **9**.

3. Dong, Q., Fu, X., Seyitliyev, D., Darabi, K., Mendes, J., Lei, L., Chen, Y.-A., Chang, C.-H., Amassian, A., Gundogdu, K., and So, F. (2022) Cavity Engineering of Perovskite Distributed Feedback Lasers. *ACS Photonics*.

4. Mizuno, H., Nishimura, T., Mekata, Y., Kurahashi, N., Odani, M., Nguyen, V.C., Inada, Y., Yamao, T., Sasaki, F., and Yanagi, H. (2021) Distributed feedback laser with methylammonium lead bromide embedded in channel-type waveguides. *Jpn. J. Appl. Phys.*, **60** (SB).

5. Roh, K., Zhao, L., and Rand, B.P. (2021) Tuning Laser Threshold within the Large Optical Gain Bandwidth of Halide Perovskite Thin Films. *ACS Photonics*, **8** (8), 2548–2554.

6. Qin, C., Sandanayaka, A.S.D., Zhao, C., Matsushima, T., Zhang, D., Fujihara, T., and Adachi, C. (2020) Stable room-temperature continuous-wave lasing in quasi-2D perovskite films. *Nature*, **585** (7823), 53–57.

7. Lei, L., Seyitliyev, D., Stuard, S., Mendes, J., Dong, Q., Fu, X., Chen, Y., He, S., Yi, X., Zhu, L., Chang, C., Ade, H., Gundogdu, K., and So, F. (2020) Efficient Energy Funneling in Quasi-2D Perovskites: From Light Emission to Lasing. *Adv. Mater.*, **1906571**, 1906571.

8. Pourdavoud, N., Haeger, T., Mayer, A., Cegielski, P.J., Giesecke, A.L., Heiderhoff, R., Olthof, S., Zaefferer, S., Shutsko, I., Henkel, A., Becker-Koch, D., Stein, M., Cehovski, M., Charfi, O., Johannes, H., Rogalla, D., Lemme, M.C., Koch, M., Vaynzof, Y., Meerholz, K., Kowalsky, W., Scheer, H., Görrn, P., and Riedl, T. (2019) Room-Temperature Stimulated Emission and Lasing in Recrystallized Cesium Lead Bromide Perovskite Thin Films. *Adv. Mater.*, 1903717.

9. Roh, K., Zhao, L., Gunnarsson, W.B., Xiao, Z., Jia, Y., Giebink, N.C., and Rand, B.P. (2019) Widely Tunable, Room Temperature, Single-Mode Lasing Operation from Mixed-Halide Perovskite Thin Films. *ACS Photonics*, **6** (12), 3331–3337.

10. Leyden, M.R., Terakawa, S., Matsushima, T., Ruan, S., Goushi, K., Auffray, M., Sandanayaka, A.S.D., Qin, C., Bencheikh, F., and Adachi, C. (2019) Distributed Feedback Lasers and Light-Emitting Diodes Using 1-Naphthylmethylamnonium Low-Dimensional Perovskite. *ACS Photonics*, **6** (2), 460–466.

11. Leyden, M.R., Matsushima, T., Bencheikh, F., and Adachi, C. (2019) Film transfer of structured organo-lead-halide perovskite for low-cost lasing applications. *Appl. Phys. Lett.*, **115** (14), 141106.

12. Bar-On, O., Brenner, P., Lemmer, U., and Scheuer, J. (2018) Micro Lasers by Scalable Lithography of Metal-Halide Perovskites. *Adv. Mater. Technol.*, **1800212**, 1800212.

13. Mathies, F., Brenner, P., Hernandez-Sosa, G., Howard, I.A., Paetzold, U.W., and Lemmer, U. (2018) Inkjet-printed perovskite distributed feedback lasers. *Opt. Express*, **26** (2), A144.

14. Gong, J., Wang, Y., Liu, S., Zeng, P., Yang, X., Liang, R., Ou, Q., Wu, X., and Zhang, S. (2017) All-

inorganic perovskite-based distributed feedback resonator. *Opt. Express*, **25** (24), A1154.

15. Jia, Y., Kerner, R.A., Grede, A.J., Rand, B.P., and Giebink, N.C. (2017) Continuous-wave lasing in an organic–inorganic lead halide perovskite semiconductor. *Nat. Photonics*, **11** (12), 784–788.

16. Harwell, J.R., Whitworth, G.L., Turnbull, G.A., and Samuel, I.D.W. (2017) Green Perovskite Distributed Feedback Lasers. *Sci. Rep.*, **7** (1), 11727.

17. Whitworth, G.L., Harwell, J.R., Miller, D.N., Hedley, G.J., Zhang, W., Snaith, H.J., Turnbull, G.A., and Samuel, I.D.W. (2016) Nanoimprinted distributed feedback lasers of solution processed hybrid perovskites. *Opt. Express*, **24** (21), 23677.

18. Brenner, P., Stulz, M., Kapp, D., Abzieher, T., Paetzold, U.W., Quintilla, A., Howard, I.A., Kalt, H., and Lemmer, U. (2016) Highly stable solution processed metal-halide perovskite lasers on nanoimprinted distributed feedback structures. *Appl. Phys. Lett.*, **109** (14), 141106.

19. Streifer, W., Scifres, D., and Burnham, R. (1975) Coupling coefficients for distributed feedback single- and double-heterostructure diode lasers. IEEE J. Quantum Electron., **11** (11), 867–873.

20. Yang, S.S., Chang, Y.-C., Yen, P.-C., and Chou, Y.-C. (2007) Effects of duty cycle on the characteristics of a composite surface-emitting organic distributed feedback laser. *J. Opt. Soc. Am. B*, **24** (8), 1857.